ChemComm

COMMUNICATION

View Article Online
View Journal

Cite this: DOI: 10.1039/d0cc00532k

Received 20th January 2020,
Accepted 11th February 2020

DOI: 10.1039/d0cc00532k

rsc.li/chemcomm

Coordination disk-type nano-Saturn complexes†

Shun-Ze Zhan, *[ac] Jing-Hong Li, [a] Guo-Hui Zhang, [a] Ming-De Li, [a] Shanshan Sun, [a] Ji Zheng, [b] Guo-Hong Ning, [b] Mian Li, [a] Dai-Bin Kuang, [d] Xu-Dong Wang [d] and Dan Li *[b]

The first coordination disk-type nano-Saturn complexes, $[Cu_{10}(Mim)_{10}]\supset C_{60}$ and $[Cu_{10}(Mim)_{10}]\supset C_{70}$ (Mim = 2-methylimidazolate), were assembled under one-pot solvothermal conditions. The highest number of 30 C–H···π interactions between the $[Cu_{10}(Mim)_{10}]$ disk and the C_{60}/C_{70} surfaces drives the formation of the nano-Saturns. The calculated interaction energy is much larger than that of most of the reported disk-type nano-Saturns. Different photoinduced charge/energy transfer mechanisms are present for both nano-Saturn systems to quench the intrinsic luminescence of the $[Cu_{10}(Mim)_{10}]$ disk.

Recently, nano-Saturn supramolecular systems (ring⊃fullerene),[1] a fullerene moiety encapsulated in the center of a nano-sized macrocycle, like the planet Saturn surrounded by its rings, have attracted tremendous attention in supramolecular chemistry due to their esthetical structures and photoinduced charge/energy transfer from the ring donor to the fullerene acceptor.[1b,c,2] To achieve a nano-Saturn, a suitable inner diameter (*ca.* 1.4 nm) for the macrocycle, a large contact area and strong synergistic supramolecular interactions between the macrocycle and the fullerene are essential. Theoretical calculations indicated that the binding energy between [10]CPP (cycloparaphenylene)/[17]cyclacene and $C_{60}/Li@C_{60}^{+}$ is larger than 100 kJ mol^{-1} because of their very matchable inner diameter and strong convex–concave π–π interactions as well as donor–acceptor interactions.[1d,3]

In a nano-Saturn system, the macrocycle exhibits belt- and disk-type shape (Scheme 1a), as suggested by Toyota *et al.*[1a] The belt-type shows convex–concave π–π interactions between the fullerene and the hoop-shaped macrocycle (Scheme 1a and Fig. S1 in the ESI†) mostly with a binding energy larger than 100 kJ mol^{-1} (Table S1 in the ESI†), such as cycloarylenes (cyclo-*p*-phenylenes,[4] cyclic paraphenyleneacetylene,[1e,5] [4]cyclochrysenylene,[6] (12,8)-[4]cyclo-2,8-anthanthrenylene,[7] and cationic cyclophanes[8]) and coordination macrocycles.[1i–k,9] In contrast, the disk-type, more like the real Saturn, has a convex-edge contact between the fullerene and the annulus disk (Scheme 1a and Fig. S1 in the ESI†), including oligothiophenes,[1c,h,10] [24]circulene,[11] cyclo-2,7-anthrylene hexamer $(C_{14}H_8)_6$,[1a,12] cyclohexabiphenylene $(C_{12}H_8)_6$,[12] and porous graphene (PG).[1f] Experimental and theoretical studies reveal that most of them bear a binding energy much lower than 60 kJ mol^{-1} (Table S1 in the ESI†), due to the much smaller contact area and weaker interactions. They contain covalent π-conjugated macrocyclic precursors (Fig. S1 in the ESI†), normally prepared by complicated organic synthesis procedures in low yield.[1a–c,e,g,5a,10a]

For metal-involved coordination nano-Saturns, only belt-type systems of copper(II) β-diketonate macrocycles,[1i,j] 3-D C_{60}/C_{70}-encapsulated coordination cages[9,13] and a new Zn_{24} metallacycle[1k] have been reported, and no disk-type nano-Saturns were obtained. It is a great challenge to construct a stable and size-fit disk-type

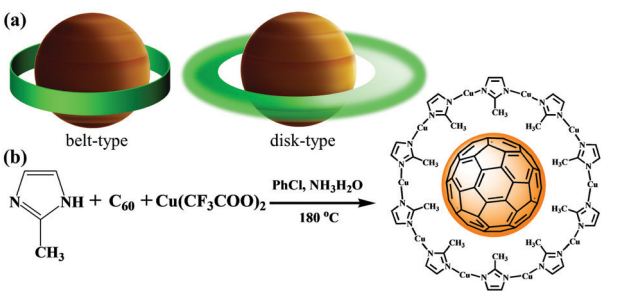

Scheme 1 Illustration of the belt- and disk-type nano-Saturn (a) and the synthesis of the coordination disk-type $[Cu_{10}(Mim)_{10}]\supset C_{60}$ nano-Saturn (b).

[a] *Department of Chemistry and Key Laboratory for Preparation and Application of Ordered Structural Materials of Guangdong Province, Shantou University, Shantou 515063, P. R. China. E-mail: szzhan@stu.edu.cn*

[b] *College of Chemistry and Materials Science, Jinan University, Guangzhou 510632, P. R. China. E-mail: danli@jnu.edu.cn*

[c] *Chemistry and Chemical Engineering Guangdong Laboratory, Shantou 515031, P. R. China*

[d] *MOE Key Laboratory of Bioinorganic and Synthetic Chemistry, Lehn Institute of Functional Materials, School of Chemistry, Sun Yat-Sen University, Guangzhou 510275, P. R. China*

† Electronic supplementary information (ESI) available: Experimental details, crystal data, physical measurements, spectra properties and theoretical calculations. CCDC 1943395–1943402. For ESI and crystallographic data in CIF or other electronic format see DOI: 10.1039/d0cc00532k

coordination macrocycle because of the intrinsic lability of coordination interactions and crowd effects in the planar disk-type coordination macrocycles, especially for the multicomponent coordination macrocycles.

Herein, we report the synthesis (details in the ESI†) and crystal structures of two nano-Saturn complexes, $[Cu_{10}(Mim)_{10}]\supset C_{60}$ (C_{60}-Saturn) and $[Cu_{10}(Mim)_{10}]\supset C_{70}$ (C_{70}-Saturn) (Mim = 2-methylimidazolate), assembled under one-pot solvothermal conditions (Scheme 1b and Fig. S2 in the ESI†). They demonstrate a real disk-type coordination nano-Saturn structure with a fullerene (C_{60}/C_{70}) encapsulated in the center of a disk-type coordination macrocyclic $[Cu_{10}(Mim)_{10}]$. The 10 methyl groups of Mim provide as high as 30 C–H$\cdots\pi$ interactions with the convex of the C_{60}/C_{70} molecule to stabilize the disk-type coordination macrocycle. The calculated interaction energy is much larger than most of the reported disk-type nano-Saturns (Table S1 in the ESI†).

Each of the two complexes is composed of a C_{60}/C_{70} molecule capsulated at the center of a $[Cu_{10}(Mim)_{10}]$ macrocycle to form a disk-type nano-Saturn (Fig. 1 and Fig. S3 in the ESI†). They are stable in air and begin to decompose until higher than 300 °C under dry N_2 flow (Fig. S5 in the ESI†). At 300 and 250 K, the C_{60}/C_{70} moiety shows a disordered occupation, possibly due to the rotation of the spherical C_{60}/C_{70} molecule. However, the rotational motion is frozen under lower temperatures (200 and 100 K), leading to an exact occupation of the C_{60}/C_{70} moiety and a different unit cell for both the complexes (Table S2 and Fig. S6 in the ESI†). For convenience, only the crystallographic data at 100 K were described. The N–Cu bond distances (1.840–1.872 Å) and the N–Cu–N bond angles (172.3°–179.4°) (Table S3 in the ESI†) are similar to those reported for $[Cu_{10}(Mim)_{10}]$.[14] 30 C–H$\cdots\pi$ cooperative interactions between 10 methyl groups and the adjacent hexagons/pentagons of the C_{60}/C_{70} surface stabilize the disk-type nano-Saturn structures. The closest distances between these H atoms and the C_{60}/C_{70} surfaces are *ca.* 3.1–3.6 Å, similar to those in the $(C_{14}H_8)_6\supset C_{60}$ system.[1a] However, the largest number of C–H$\cdots\pi$ interactions furnishes much stronger host–guest supramolecular interactions than those reported for nano-Saturn systems. Compared with the two-fold disordered Mim ligand in the $[Cu_{10}(Mim)_{10}]\supset p$-xylene/naphthalene,[14b] all the methyl groups of Mim are pointed to the fullerene center without disorder to form a coplanar disk, which is believed to relate to the stronger C–H$\cdots\pi$ cooperative interactions in the two nano-Saturns than in the $[Cu_{10}(Mim)_{10}]\supset p$-xylene/naphthalene.[14]

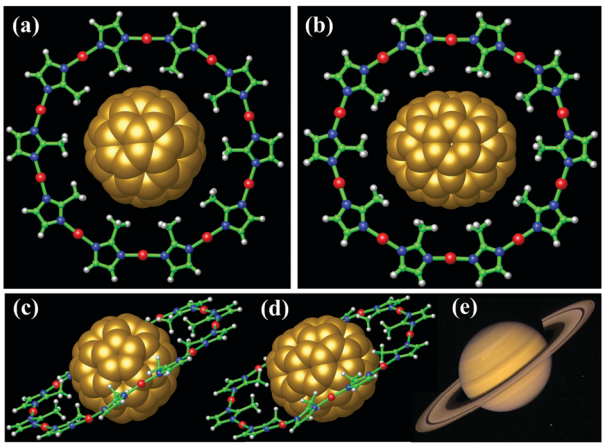

Fig. 1 The top view (a and b) and side view (c and d) of the C_{60} (a and c) and C_{70} (b and d) -Saturns and comparison with the real Saturn from the side view (e).

A very round $[Cu_{10}(Mim)_{10}]$ macrocycle is presented in the C_{60}-Saturn due to the spherical C_{60} molecule, in which the opposite Mim center distances are very similar from 19.17 to 19.63 Å (Table S3 in the ESI†). However, an elliptic disk is shown in the C_{70}-Saturn because the elliptical C_{70} prefers the "standing" orientation but not lying/half-lying in the cavity, which means that the 5-fold symmetry axis of C_{70} almost coincides with the macrocycle plane, or the long axis of C_{70} is perpendicular to the macrocycle axis, as reported in the belt-type C_{70}-Saturn.[1j,15] The largest opposite Mim center distance is about 20.03 Å, whereas the shortest one is 18.96 Å. Additionally, the bulky C_{70} causes much closer contact distances between the macrocycle and the C_{70} surface and slightly longer N–Cu bond distances (1.853–1.872 Å) than that (1.840–1.856 Å) in the C_{60}-Saturn. The closest distance between the $C(CH_3)$ atoms and the center of C_{70} is about 6.844(4) Å, much shorter than 7.077(2) Å in the C_{60}-Saturn.

The nano-Saturns are interlaced through different Cu$\cdots$Cu interactions 3.021(1)–3.700(1) Å among the $[Cu_{10}(Mim)_{10}]$ macrocycles to form similar 3-D packing structures (Fig. S7 and S8 in the ESI†). For example, these shorter Cu$\cdots$Cu distances (3.021(1) and 3.166(1) Å for the C_{60}-Saturn and 3.037(1)–3.129(4) Å for the C_{70}-Saturn) extend the $[Cu_{10}(Mim)_{10}]$ macrocycles to a kind of 2-D sheet, which are connected by the largest Cu$\cdots$Cu distances (3.330(1) Å for the C_{60}-Saturn, 3.579(1) and 3.700(1) Å for the C_{70}-Saturn) to form the 3-D packing structures (Fig. S7 and S8 in the ESI†). The packing of the macrocycles provides a 1-D channel with a 7.9 Å × 8.7 Å window (Fig. S7e and S8e in the ESI†). However, it is too small to allow C_{60}/C_{70} departing/entering the crystal freely, consistent with the experimental results: soaking the crystal samples into toluene, xylene or chlorobenzene for about 1 week did not result in color change of the solvents.

To explore the interactions between the C_{60}/C_{70} and the $[Cu_{10}(Mim)_{10}]$, DFT calculations were carried out to optimize the two nano-Saturn molecules and evaluate the interaction energy. The structure of the free $[Cu_{10}(Mim)_{10}]$ macrocycle was also optimized. The optimized C_{60}-Saturn shows high similarity to the measured structure (Fig. S9 in the ESI†), whereas the $[Cu_{10}(Mim)_{10}]$ in the optimized C_{70}-Saturn is severely distorted due to the bulky C_{70} (Fig. S10 in the ESI†). The optimized free $[Cu_{10}(Mim)_{10}]$ shows a coplanar structure for the Cu atoms; however, the Mim planes are severely deviated from the Cu plane to show much larger dihedral angles (18.18°–50.16°) than those in the C_{60}-Saturn (Table S3 and Fig. S11e in the ESI†) due to the steric crowding among these methyl groups, which implies strong C–H$\cdots\pi$ interactions between the macrocycle and the C_{60} surface. The interaction energy ΔE_{int} was calculated to be −85.25 and −116.07 kJ mol^{-1} for the C_{60}- and C_{70}-Saturn, respectively, much larger than those reported for covalent

Table 1 Energy decomposition analysis (kJ mol^{-1}) for the C_{60}- and C_{70}-Saturn, respectively

Nano-Saturn	ΔE_{int}	ΔE_{Pauli}	ΔE_{elstat}	ΔE_{orb}	ΔE_{disp}
C_{60}-Saturn	−85.25	57.48	−13.12, 9.19%	−14.56, 10.20%	−115.05, 80.61%
C_{70}-Saturn	−116.07	136.83	−47.13, 18.64%	−31.70, 12.53%	−174.07, 68.83%

$\Delta E_{int} = \Delta E_{Pauli} + \Delta E_{elstat} + \Delta E_{orb} + \Delta E_{disp}$.

disk-type nano-Saturns (Table 1 and Table S1 in the ESI†). The energy decomposition analysis (EDA)[16] indicates that ΔE_{disp} contributes most (larger than 68%) for the stabilizing energy (ΔE_{elstat} + ΔE_{orb} + ΔE_{disp}), suggesting that van der Waals (dispersion) forces dominate the host–guest interactions. However, both the electrostatic and covalent character demonstrated by ΔE_{elstat} and ΔE_{orb} contribute no more than 32% for the stabilizing energy. It is not surprising because the strong electron-withdrawing/pulling group is absent in such inclusion complexes. The methyl group is a weak electron donor for the C–H$\cdots\pi$ interactions, significantly different from those of cyclophane-C_{60},[8] CPP-Li@C_{60}^{+1}[d] and porphyrin-C_{60}[9] with strong electrostatic and covalent character. Careful comparison of the energy decomposition results reveals that the C_{70}-Saturn shows not only larger ΔE_{int} but also all the decomposed terms (in particular, the ΔE_{Pauli}). This may be reasonably assigned to the much closer ring-planet distances caused by the bulkier C_{70} than C_{60}.

The spatial charge distributions over the C_{60}/C_{70} surfaces are shown by the molecular electrostatic potential (MEP) surfaces, giving further understanding in the electrostatic character of the interaction. By comparing the MEP surface of the free C_{60}/C_{70}, a positive region lies on the belt of the C_{60}/C_{70} surfaces surrounded by methyl groups (Fig. 2a, b and Fig. S12 in the ESI†), indicating that weak electrostatic interactions cannot be excluded, as evidenced by the small ΔE_{elstat}.

TD-DFT calculation reveals that the occupied frontier orbitals are localized in the macrocycle and the unoccupied ones are in the C_{60}/C_{70} moiety (Fig. 2c, d and Fig. S13, S14 in the ESI†).

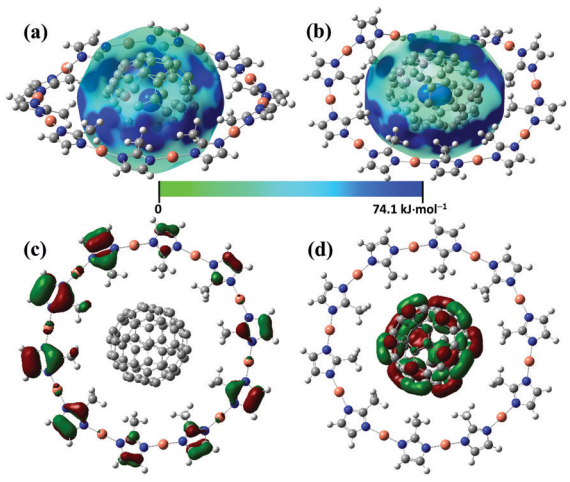

Fig. 2 Calculation results to show: MEP surfaces at C_{60} and C_{70} in the C_{60}-Saturn (a) and C_{70}-Saturn (b) from the side view (at 0.015 a.u.); the spatial contours of the HOMO (c) and the LUMO (d) for the C_{60}-Saturn (isovalue = 0.015).

The calculated energy gap between the HOMO and the LUMO is 2.33 eV (533 nm) and 2.31 eV (537.7 nm) for the C_{60}- and C_{70}-Saturn, respectively. The low energy gap provides a possibility for photoinduced charge transfer from the macrocycle to the fullerene.

Both nano-Saturn complexes do not emit in the visible region. However, the $[Cu_{10}(Mim)_{10}]\supset p$-xylene complex shows photoluminescence with λ_{em}^{max} = 515 nm (λ_{ex}^{max} = 280 nm) at room temperature based on ^{3}[MLCT] enhanced by cuprophilicity.[14] Transient absorption (TA) spectroscopy[17] was performed to explore the possible photoinduced charge/energy interplay between C_{60}/C_{70} and the macrocycle (Fig. 3). Due to their poor solubility in common solvents and serious absorption of the pure solid, KBr disks with 1% of the complexes were used for measurements.

Both complexes show similar broad absorption covering the whole UV-Vis region (Fig. S15 in the ESI†). Noticeably, the absorption curve of C_{60}-Saturn gives a characteristic absorption of the anionic C_{60}^- at 1080 nm[18] (Fig. S15b in the ESI†), indicating the presence of charge transfer from the $[Cu_{10}(Mim)_{10}]$ to the C_{60} planet. The charge separation is also evidenced by the TA spectra in the NIR region with a peak at around 1080 nm under photoexcitation at λ = 350 nm, produced in 410 fs then followed by charge recombination in several nanoseconds. Additionally, a weak peak at about 920 nm corresponding to the singlet $^1C_{60}{}^*$[19] is observed, which is believed to be directly photoexcited (Fig. 3a and b).

In contrast, no charge transfer was detected for the C_{70}-Saturn because of the lack of the characteristic absorption of the C_{70}^- at 1370 nm[20] (Fig. 3c, d and Fig. S15c in the ESI†).

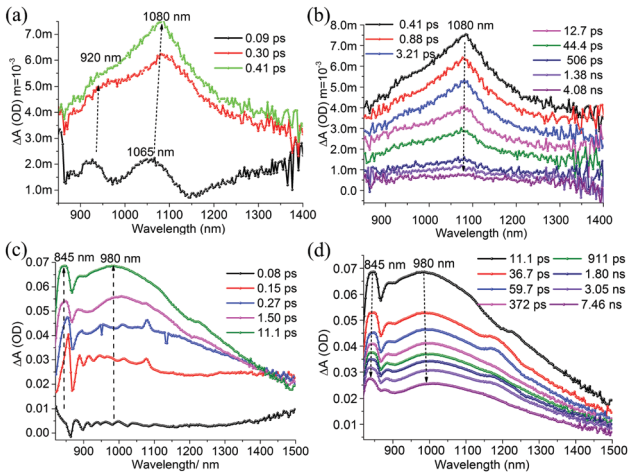

Fig. 3 TA spectra in the NIR region of the solid C_{60}-Saturn (a and b) and C_{70}-Saturn (c and d) in a KBr disk (1% concentration).

Its TA spectra in the NIR region display a strong absorption at 980 nm with a narrow peak at 845 nm in 11.1 ps (Fig. 3c), which originated from the triplet $^3C_{70}$* [20a] and the singlet $^1C_{70}$*,[19] respectively. They decayed simultaneously in several nanoseconds (Fig. 3d), consistent with the reported decay time of $^3C_{70}$*, implying a fast dynamic balance between the $^1C_{70}$* and $^3C_{70}$*. The triplet $^3C_{70}$* and the singlet $^1C_{70}$* can be produced by direct photoexcitation; however, the luminescence quenching of $[Cu_{10}(Mim)_{10}]$ in the C_{70}-Saturn reveals the possible energy transfer from the excited $[Cu_{10}(Mim)_{10}]$ to produce the excited C_{70}.

Accordingly, the quenching mechanisms for the excited macrocycle $[Cu_{10}(Mim)_{10}]$ are significantly different in both complexes. Similar to the most reported nano-Saturn, the C_{60}-Saturn displays a significant charge transfer from the macrocycle to the C_{60} to form a charge-separated state upon photoexcitation.[1b,c,2] However, energy transfer than charge transfer happens in the C_{70}-Saturn. This reveals a controlling effect of the C_{60}/C_{70}-fullenene on the charge/energy transfer in the nano-Saturn systems. However, the exact reasons for the significantly different photophysics are unclear at this stage.

In conclusion, two coordination disk-type nano-Saturn complexes, $[Cu_{10}(Mim)_{10}]\supset C_{60}$ and $[Cu_{10}(Mim)_{10}]\supset C_{70}$, were assembled under one-pot solvothermal conditions. The macrocyclic $[Cu_{10}(Mim)_{10}]$ provides an accurate shape and size for the formation of a disk-type Saturn. Multiple C–H$\cdots\pi$ interactions between the macrocyclic disk and the C_{60}/C_{70} surfaces make dominant contributions for the stabilization of the disk-type nano-Saturn. The calculated interaction energies are significantly larger than other disk-type organic nano-Saturns, even near to those belt-type analogues. Charge/energy transfer processes found in the C_{60}/C_{70}-Saturn are responsible for quenching the intrinsic luminescence of the coordination macrocycle. This work not only provides an efficient one-pot method to prepare a disk-type coordination nano-Saturn offering a versatile nano-Saturn system but also helps for a better understanding of the host–guest supramolecular interactions between the fullerene and the macrocycle.

This work was financially supported by the National Natural Science Foundation of China (No. 21975104 and 21471094), the Major Program of Guangdong Basic and Applied Research (No. 2019B030302009), and the Guangdong Basic and Applied Basic Research Foundation (No. 2019A1515012162).

Conflicts of interest

There are no conflicts to declare.

Notes and references

1 (*a*) Y. Yamamoto, E. Tsurumaki, K. Wakamatsu and S. Toyota, *Angew. Chem., Int. Ed.*, 2018, **57**, 8199; (*b*) Y. Xu, R. Kaur, B. Wang, M. B. Minameyer, S. Gsanger, B. Meyer, T. Drewello, D. M. Guldi and M. von Delius, *J. Am. Chem. Soc.*, 2018, **140**, 13413; (*c*) H. Shimizu, K. H. Park, H. Otani, S. Aoyagi, T. Nishinaga, Y. Aso, D. Kim and M. Iyoda, *Chem. – Eur. J.*, 2018, **24**, 3793; (*d*) H. U. Rehman, N. A. McKee and M. L. McKee, *J. Comput. Chem.*, 2016, **37**, 194; (*e*) T. Kawase, K. Tanaka, N. Fujiwara, H. R. Darabi and M. Oda, *Angew. Chem., Int. Ed.*, 2003, **42**, 1624; (*f*) C. Chakravarty, B. Mandal and P. Sarkar, *J. Phys. Chem. C*, 2018, **122**, 15835; (*g*) M. Iyoda, H. Shimizu, S. Aoyagi, H. Okada, B. Zhou and Y. Matsuo, *Can. J. Chem.*, 2017, **95**, 315; (*h*) J. D. Cojal González, M. Iyoda and J. P. Rabe, *Nat. Commun.*, 2017, **8**, 14717; (*i*) C. Pariya, C. R. Sparrow, C. K. Back, G. Sandi, F. R. Fronczek and A. W. Maverick, *Angew. Chem., Int. Ed.*, 2007, **46**, 6305; (*j*) J. K. Cherutoi, J. D. Sandifer, U. R. Pokharel, F. R. Fronczek, S. Pakhomova and A. W. Maverick, *Inorg. Chem.*, 2015, **54**, 7791; (*k*) C. R. Göb, A. Ehnbom, L. Sturm, Y. Tobe and I. M. Oppel, *Chem. – Eur. J.*, 2020, DOI: 10.1002/chem.201905390.

2 S. Hitosugi, K. Ohkubo, R. Iizuka, Y. Kawashima, K. Nakamura, S. Sato, H. Kono, S. Fukuzumi and H. Isobe, *Org. Lett.*, 2014, **16**, 3352.

3 (*a*) I. Gonzalez-Veloso, J. Rodriguez-Otero and E. M. Cabaleiro-Lago, *Phys. Chem. Chem. Phys.*, 2018, **20**, 27791; (*b*) K. Yuan, C.-H. Zhou, Y.-C. Zhu and X. Zhao, *Phys. Chem. Chem. Phys.*, 2015, **17**, 18802.

4 T. Iwamoto, Y. Watanabe, T. Sadahiro, T. Haino and S. Yamago, *Angew. Chem., Int. Ed.*, 2011, **50**, 8342.

5 (*a*) T. Kawase, K. Tanaka, Y. Seirai, N. Shiono and M. Oda, *Angew. Chem., Int. Ed.*, 2003, **42**, 5597; (*b*) T. Kawase, N. Fujiwara, M. Tsutumi, M. Oda, Y. Maeda, T. Wakahara and T. Akasaka, *Angew. Chem., Int. Ed.*, 2004, **43**, 5060.

6 H. Isobe, S. Hitosugi, T. Yamasaki and R. Iizuka, *Chem. Sci.*, 2013, **4**, 1293.

7 T. Matsuno, S. Sato and R. I. Isobe, *Chem. Sci.*, 2015, **6**, 909.

8 J. C. Barnes, E. J. Dale, A. Prokofjevs, A. Narayanan, I. C. Gibbs-Hall, M. Juricek, C. L. Stern, A. A. Sarjeant, Y. Y. Botros, S. I. Stupp and J. F. Stoddart, *J. Am. Chem. Soc.*, 2015, **137**, 2392.

9 J. Song, N. Aratani, H. Shinokubo and A. Osuka, *J. Am. Chem. Soc.*, 2010, **132**, 16356.

10 (*a*) H. Shimizu, J. D. Cojal Gonzalez, M. Hasegawa, T. Nishinaga, T. Haque, M. Takase, H. Otani, J. P. Rabe and M. Iyoda, *J. Am. Chem. Soc.*, 2015, **137**, 3877; (*b*) S. Q. Zhang, Z. Y. Liu, W. F. Fu, F. Liu, C. M. Wang, C. Q. Sheng, Y. F. Wang, K. Deng, Q. D. Zeng, L. J. Shu, J. H. Wan, H. Z. Chen and T. P. Russell, *ACS Nano*, 2017, **11**, 11701.

11 S. Kigure and S. Okada, *Jpn. J. Appl. Phys.*, 2015, **54**, 06FF01.

12 S. Kigure, H. Omachi, H. Shinohara and S. Okada, *J. Phys. Chem. C*, 2015, **119**, 8931.

13 D. Canevet, E. M. Perez and N. Martin, *Angew. Chem., Int. Ed.*, 2011, **50**, 9248.

14 (*a*) Y. Wang, C.-T. He, Y.-J. Liu, T.-Q. Zhao, X.-M. Lu, W.-X. Zhang, J.-P. Zhang and X.-M. Chen, *Inorg. Chem.*, 2012, **51**, 4772; (*b*) X.-C. Huang, J.-P. Zhang and X.-M. Chen, *J. Am. Chem. Soc.*, 2004, **126**, 13218.

15 K. Yuan, Y.-J. Guo and X. Zhao, *J. Phys. Chem. C*, 2015, **119**, 5168.

16 (*a*) M. V. Hopffgarten and G. Frenking, *Wiley Interdiscip. Rev.: Comput. Mol. Sci.*, 2012, **2**, 43; (*b*) L. Zhao, M. von Hopffgarten, D. M. Andrada and G. Frenking, *Wiley Interdiscip. Rev.: Comput. Mol. Sci.*, 2018, **8**, e1345; (*c*) T. Ziegler and A. Rauk, *Theor. Chim. Acta*, 1977, **46**, 1.

17 M. D. Li, N. K. Wong, J. Xiao, R. Zhu, L. Wu, S. Y. Dai, F. Chen, G. Huang, L. Xu, X. Bai, M. R. Geraskina, A. H. Winter, X. Chen, Y. Liu, W. Fang, D. Yang and D. L. Phillips, *J. Am. Chem. Soc.*, 2018, **140**, 15957.

18 D. R. Lawson, D. L. Feldheim, C. A. Foss, P. K. Dorhout, C. M. Elliott, C. R. Martin and B. Parkinson, *J. Electrochem. Soc.*, 1992, **139**, L68.

19 M. Lee, O.-K. Song, J.-C. Seo and D. Kim, *Chem. Phys. Lett.*, 1992, **196**, 325.

20 (*a*) R. V. Bensasson, T. Hill, C. Lambert, E. J. Land, S. Leach and T. G. Truscott, *Chem. Phys. Lett.*, 1993, **206**, 197; (*b*) D. R. Lawson, D. L. Feldheim, C. A. Foss, P. K. Dorhout, C. M. Elliott, C. R. Martin and B. Parkinson, *J. Phys. Chem.*, 1992, **96**, 7175.

